The Counter-Streaming Instability in Dwarf Ellipticals with Off-Center Nuclei[1]

Sven De Rijcke[2]

Sterrenkundig Observatorium, Universiteit Gent, Krijgslaan 281, S9, B-9000 Gent, Belgium

sven.derijcke@UGent.be

Victor P. Debattista

Institut für Astronomie, ETH Hönggerberg, HPF G4.2, CH-8093 Zürich, Switzerland

debattis@phys.ethz.ch

ABSTRACT

In many nucleated dwarf elliptical galaxies (dE,Ns), the nucleus is offset by a significant fraction of the scale radius with respect to the center of the outer isophotes. Using a high-resolution N-body simulation, we demonstrate that the nucleus can be driven off-center by the $m = 1$ counter-streaming instability, which is strong in flattened stellar systems with zero rotation. The model develops a nuclear offset of the order of one third of the exponential scale-length. We compare our numerical results with photometry and kinematics of FCC046, a Fornax cluster dE,N with a nucleus offset by $1''.2$; we find good agreement between the model and FCC046. We also discuss mechanisms that may cause counter-rotation in dE,Ns and conclude that the destruction of box orbits in an initially triaxial galaxy is the most promising.

Subject headings: galaxies: dwarf— galaxies: evolution— galaxies: individual (FCC046)— galaxies: kinematics and dynamics— galaxies: structure— galaxies: nuclei

---

[1]Based partly on observations collected at the European Southern Observatory, Paranal, Chile (ESO Large Program 165.N 0115)

[2]Research Postdoctoral Fellow of the Fund for Scientific Research - Flanders (Belgium)(F.W.O.)

1. Introduction

Dwarf elliptical galaxies (dEs), faint, low-surface brightness galaxies with smooth elliptical isophotes, are the most common type of galaxy in clusters and groups of galaxies (see Binggeli & Ferguson (1994)). In hierarchical models of cosmological structure formation, dwarf galaxies form first and subsequently merge to form larger galaxies. Understanding their formation and evolution is therefore vital to a complete picture of structure formation. There is evidence that dEs constitute a heterogenous class of objects, kinematically (rotating versus unrotating, Geha *et al.* (2003)), chemically (Michielsen *et al.* 2003) and morphologically (Barazza *et al.* 2002). About half of the dEs harbor a central bright nucleus and are called nucleated dEs (dE,Ns). dE,Ns appear to be significantly older than normal ellipticals and non-nucleated dEs (Rakos & Schombert 2003); upon tidal stripping, their nuclei have been suggested as sources of both the recently discovered ultra compact dwarfs (Phillipps *et al.* 2001) and massive globular clusters like ωCen (Gnedin *et al.* 2002). In $\sim 20\%$ of Virgo dE,Ns, the nucleus is significantly displaced with respect to the center of the outer isophotes, typically by $\sim 1''$ (~ 100 pc) (Binggeli *et al.* 2000). There is a tendency for the displacement to increase with decreasing surface brightness but no relation between nuclear displacement and any other structural or environmental parameter has been found.

Various models have been proposed to explain these offset nuclei. In this Letter, we investigate whether the lopsided ($m = 1$) counter-streaming instability can reproduce a dE,N with an off-center nucleus. This instability has been known since Zang & Hohl (1978), and been studied analytically (Sawamura 1988; Palmer & Papaloizou 1990) and with N-body simulations (Merritt & Stiavelli 1990; Levison *et al.* 1990; Sellwood & Merritt 1994; Sellwood & Valluri 1997). Sellwood & Valluri (1997) do not detect it in systems rounder than E6, which is mainly due to their rounder models being stabilized by a higher radial pressure. On the other hand, Merritt & Stiavelli (1990) find lopsidedness developing in systems as round as E1 but with negligible radial pressure. Partial rotation only introduces a pattern speed in an otherwise purely growing instability; simulations find that the lopsidedness produced by the instability is long-lived.

We use a realistic multi-component N-body model to generate a lopsided system which we then compare with observations. In Section 2, we present the N-body model and in Section 3 we compare it with photometry and kinematics of FCC046, an example of such a dE,N with an offset nucleus. In Section 4, we discuss ways in which counter-rotation may arise in dE,Ns.

2. N-body simulation

We have been using N-body simulations to explore the counter-streaming instability as a mechanism for producing lopsided dE,Ns. We have performed both fully self-consistent simulations with live nucleus, disk and halo run on a tree code, and restricted simulations with rigid halos run on a grid code; both types of simulations will be presented elsewhere. Here we present only one simulation which happens to match FCC046 best, consisting of live disk and nucleus components inside a rigid halo. The rigid halo was represented by a spherical logarithmic potential with core-radius r_{c} and asymptotic circular velocity v_0. The initial disk was modeled by an exponential disk of mass M_{d}, scale-length R_{d}, Gaussian thickness z_{d} and truncated at R_{t}. The nucleus of mass M_{n} was generated by iteratively integrating a distribution function in the global potential (Prendergast & Tomer 1970). We used a distribution function of the form $f(\vec{x},\vec{v}) \propto \left\{[-E(\vec{x},\vec{v})]^{1/2} - [-E_{\mathrm{max}}]^{1/2}\right\}$. Here $E_{\mathrm{max}} = \Phi_{\mathrm{tot}}(r_{\mathrm{n}})$, the total potential at the nucleus truncation radius, r_{n}, in the disk mid-plane. Initial disk kinematics were set up using the epicyclic approximation to give Toomre $Q = 1.3$. Vertical equilibrium was obtained by integrating the vertical Jeans equation. The disk and nucleus were represented by 36.8×10^5 and 3.2×10^5 equal-mass particles, respectively. After setup, we switched the direction of the velocity for half the particles, producing an unrotating disk and a rotating nucleus. We used a quiet start (Sellwood 1983) to cancel spurious momenta and angular momenta.

In our units, where $R_{\mathrm{d}} = M(= M_{\mathrm{n}} + M_{\mathrm{d}}) = G = 1$, which give a unit of time $(R_{\mathrm{d}}^3/GM)^{1/2}$, we set $z_{\mathrm{d}} = 0.2$, $R_{\mathrm{t}} = 5$, $r_{\mathrm{n}} = 0.78$, $r_{\mathrm{c}} = 5$ and $v_0 = 0.648$. The simulation was run on a 3-D cylindrical polar grid code (described in Sellwood & Valluri (1997)) with $N_R \times N_\phi \times N_z = 60 \times 64 \times 225$. The vertical spacing of the grid planes was $\delta z = 0.0125$. We used Fourier terms up to $m = 8$ in the potential, which was softened with the standard Plummer kernel, of softening length $\epsilon = 0.0125$. Time integration was performed with a leapfrog integrator using a fixed time-step $\delta t = 0.006$. To scale units to FCC046, we note that its surface-brightness profile declines exponentially with scale-length $R_{\mathrm{d}} = 4\farcs1 \approx 0.4$ kpc. We estimated the stellar mass of FCC046 at $M \approx 1.0 \times 10^9 M_\odot$, given a B-band total luminosity $L_B = 2 \times 10^8 L_{B,\odot}$ and using a B-band mass-to-light ratio $M/L_B \approx 5 M_\odot/L_{B,\odot}$, typical for an old (15 Gyr), rather metal-poor ([Fe/H]$= -0.5$) stellar population. With this scale-length and mass, the unit of time corresponds to $(R_{\mathrm{d}}^3/GM)^{1/2} \approx 4$ Myr and the velocity unit becomes $(GM/R_{\mathrm{d}})^{1/2} \approx 100$ km/s.

Fig. 1.— Panel **a**: a B-band image of FCC046; panel **b**: the surface brightness of the N-body model at $t = 150$. The isophotes are spaced by 1 mag/arcsec^2 with the $\mu_B = 24$ mag/arcsec^2 isophote drawn in white. Panels **c** and **d**: the model's velocity field and the velocity dispersion field, respectively. The velocity field perturbations have an $m = 2$ symmetry and range between -0.06 (black) and $+0.06$ (white), corresponding to $\pm 0.1 \times v_{\rm circ}$.

The global lopsidedness of the model, as measured by the amplitude of the $m = 1$ term in a Fourier expansion of the surface density, rose exponentially with time, saturating at $t \simeq 70$, for an e-folding time $\tau = 5.67$. The angular momentum of the disk and the orbital angular momentum of the nucleus increase at the expense of the nucleus's internal (rotational) angular momentum. By the end of the simulation, the nucleus has lost approximately 20 % of its initial internal angular momentum. The resulting orbital velocity of the nucleus ($v_{\rm nuc} \approx 0.01$) is, however, only a few percent of the local circular velocity ($v_{\rm circ} \approx 0.35$), so that dynamical friction against a live dark matter halo is not likely to damp the instability, as is also borne out by the live halo simulations.

3. FCC046: a case study

FCC046 is an $m_B = 15.99$ dE4,N in the Fornax cluster. Photometry and long-slit spectra, with an instrumental broadening $\sigma_{\rm instr} = 30$ km/s, in the wavelength region containing the strong absorption lines of the near-infrared CaII triplet, were observed at the VLT with FORS2 in November 2001 (photometry) and 2002 (spectroscopy). Seeing conditions were typically $0\farcs8$ FWHM. A detailed analysis of the photometry has been presented in De Rijcke *et al.* (2003b), while details of the kinematics of FCC046 will be presented elsewhere. Additionally, the HST archives contain WFPC2 images of FCC046 in the filters F814W and F555W. Availability of all these data was the sole reason for selecting this object.

FCC046 contains a bright nucleus, which is displaced by $1\farcs2$ with respect to the outer isophotes, or 30% of $R_{\rm d}$. The lopsidedness involves not just the nucleus, but extends to $\sim 2R_{\rm d}$. Color maps show no traces of large amounts of dust but suggest the presence of a blue stellar population. The Hα image reveals ionized emission regions, evidence for ongoing star formation, within $\sim 1R_{\rm d}$. The position of the blue stellar population does not coincide with the lopsidedness of FCC046 and is not likely to be the cause of it (although it may be a consequence of it). FCC046 is in the outskirts of the Fornax cluster; its nearest neighbors are dwarfs over 100 kpc (in projection) away, and the nearest large galaxy is > 200 kpc distant. Interactions are therefore not likely to account for its morphology, unless a weakly damped mode has been excited (Weinberg 1994). The kinematics of FCC046 (mean velocity and velocity dispersion) were extracted from the spectra following the method discussed in De Rijcke *et al.* (2003a). Despite its E4 flattening, the main body of FCC046 has zero mean rotation. The lack of rotation excludes the possibility that the eccentric instability (Adams *et al.* 1989; Miller & Smith 1992; Taga & Iye 1998) is responsible for the lopsidedness.

The nucleus is resolved by HST; it has a FWHM$= 0\farcs27$, significantly larger than the FWHM$= 0\farcs15$ of the stars in the same image, and therefore cannot be a foreground star.

The nucleus has the same systemic velocity as the galaxy which rules out a chance projection of a background object. It comprises ~ 10 % of the B-band luminosity of FCC046 and is therefore probably quite massive. We can use the fact that the outer isophotes of the N-body model do not move appreciably and their center coincides with the model's center-of-mass (COM) to estimate the relative mass-to-light (M/L) ratios of the disk and nucleus. In order for the mean position of the B-band light distribution to coincide with the COM, the M/L ratio of the nucleus has to be less than half that of the disk. If the disk consists of an old, metal-poor population with $M/L_B \approx 5M_\odot/L_{B,\odot}$, this would mean that the nucleus has $M/L_B < 2M_\odot/L_{B,\odot}$, typical for a very young stellar population (age $< 2-3$ Gyr). This is consistent with the blue color of the nucleus and its strong Pa absorption (Michielsen *et al.* 2003). The rotation axis of the nucleus is not aligned with that of the galaxy's main body, showing evidence for minor axis rotation with an amplitude of ≈ 5 km/s.

The surface density, the velocity field and the velocity dispersion field of the N-body model at $t = 150$ are presented in Fig. 1. The viewing angle and the spatial scale were chosen such that the model's surface density gives a fair approximation to the B-band image of FCC046. The nucleus is offset by $\sim 1''$ to the south-west with respect to the outer isophotes and, in response, there is an excess in the disk density to the north-east, as in FCC046. Clearly, the instability engenders a global response of the whole stellar system. In Fig. 2, we compare the surface photometry of FCC046 with the N-body model (convolved with a Gaussian to mimic the seeing conditions of the observations) in greater detail. Simply shifting the magnitude zero-point of the N-body model and applying the same spatial scale as in Fig. 1 sufficed to match the surface brightness profile of FCC046. As in FCC046, the isophote centers of the model oscillate along the major axis; in the model this keeps the total center-of-mass fixed. Just outside the nucleus, the density contours have a distorted shape which, in projection, results in the isophotes being flatter (around $\sim 5''$ in FCC046 and around $\sim 3''$ in the model) than at larger radii. On the whole, the model successfully reproduces gross features in the surface photometry of FCC046.

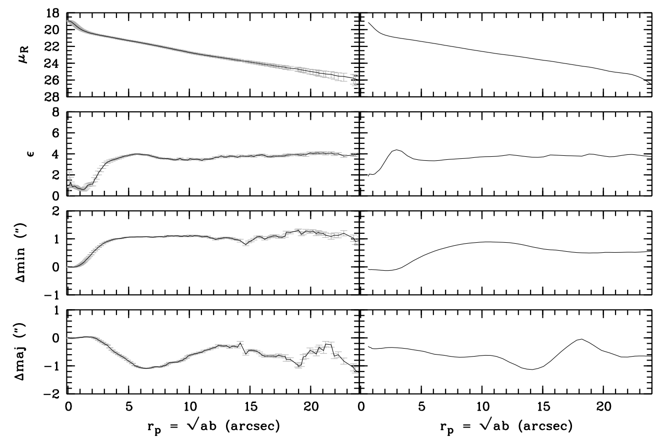

Fig. 2.— Surface photometry of FCC046 (left panels), compared with the N-body model (right panels). a and b are respectively the semi-major and minor axes of the isophotes. In the top panels, the R-band surface brightness (in mag/arcsec^2) of FCC046 is compared with that of the model. In the next panels, the ellipticity $\epsilon = 10(1 - b/a)$ of the isophotes is shown. In the bottom panels, the position of the center of the isophotes is presented. Δmaj and Δmin (in arcseconds) quantify the position of the isophotes along the major and minor axes, centered on the nucleus.

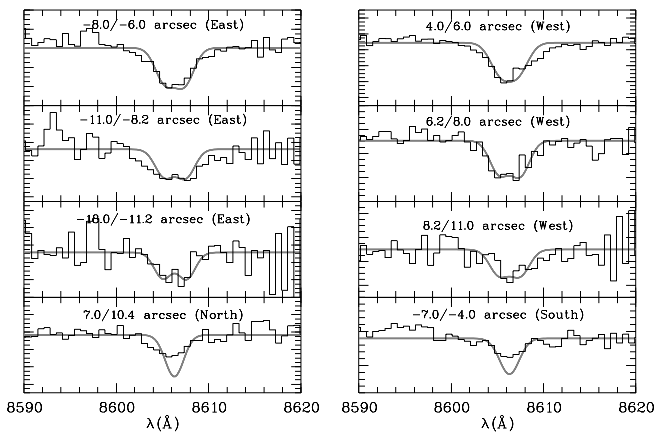

Fig. 3.— Part of the spectrum of FCC046, around the strongest CaII absorption line. The radial bins over which the spectrum has been summed to boost the S/N are indicated in the figure (left column, top three panels: along the major axis, towards east; right column, top three panels: along the major axis, towards west; bottom panels: along minor axis, towards north (left column) and towards south (right column)). Radius is measured from the nucleus. Observed spectrum: black line; model spectrum: grey line (see text for details). This absorption line appears split into two distinct lines, separated by 70 ± 25 km/s, in the outermost major axis spectra. The S/N in these panels varies from 5-10 to 20-25; adjacent spectra from the left and right columns have comparable S/N. The minor-axis spectra have the same continuum level as the outermost major-axis spectra. Clearly, the CaII line does not appear split in the minor-axis spectra. The model reproduces rather well the major-axis line width and the observed line-splitting.

Fig. 1 shows that, while the model's mean velocity is zero, bi-symmetric perturbations of order ~ 0.06 are present. The velocity dispersion profile is asymmetric, rising less rapidly towards the left side of the model, in the direction of the light excess. The apparent flattening of FCC046 and its zero mean rotation already hint at two equal-mass counter-streaming stellar populations. Although at the limit of what can be done, given the spectral resolution and the low S/N-ratio of the data, the strongest CaII absorption line in the major-axis spectrum appears split into two distinct lines (see Fig. 3), separated by 70 ± 25 km/s; the other, weaker, lines have much lower S/N-ratios. This absorption line is unaffected by the bright sky OH-emission lines. (If a badly removed sky line were the cause of the line-splitting, it would also manifest itself in the center of the galaxy and in the minor axis spectrum, which is not the case.) What is particularly compelling about these data is that the apparent bimodality is present (and absent) where the model predicts it should be (before the signal disappears in the noise), and that we see similar splitting in three different spatial bins. To illustrate this, in Fig. 3 we plot the observed spectrum and the model spectrum, consisting of a flat continuum and a very narrow (δ-function) absorption line, broadened with the FORS2 instrumental profile and the model's line-of-sight velocity distribution (LOSVD), summed over the same spatial bins as the observed spectrum. We did not use an observed stellar template since the width of the individual LOSVD peaks is smaller than one FORS2 pixel, making an accurate calculation of a synthetic galaxy spectrum impossible. Except for underestimating the minor-axis velocity dispersion, the model reproduces rather well the major-axis line widths and the observed line-splitting.

However, these observations, while very suggestive, need to be corroborated at higher spectral resolution to resolve the two peaks in the LOSVDs. In Fig. 4, we present a mosaic of LOSVDs at different points in the model. Moving out along the major axis, the LOSVDs become more double-peaked due to the increasing velocity separation between the two counter-streaming stellar populations and the declining velocity dispersion. The small velocity-field perturbations of Fig. 1 are reflected here in the LOSVDs being slightly asymmetric. Although the details of the LOSVD field in Fig. 4 are model-dependent, an observational confirmation of its salient features would lend considerable support to the hypothesis that the counter-streaming instability is responsible for off-center nuclei in dE,Ns.

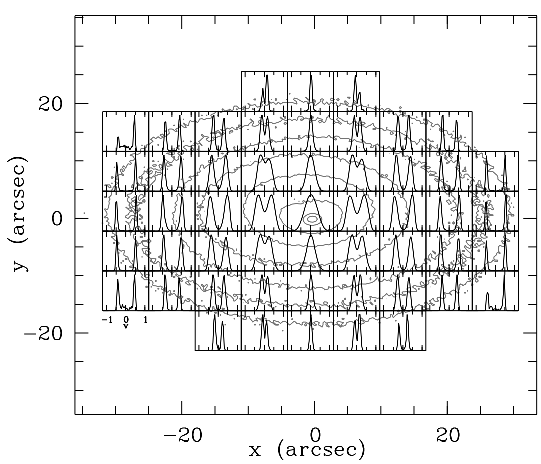

Fig. 4.— A mosaic of the LOSVDs at different points in the projected model (the middle panel is centered on the center of the outer isophotes). Big and small tickmarks indicate a velocity $v = \pm 1$ and $v = \pm 0.5$, respectively, as indicated below the leftmost panel. The isophotes of the model, separated by 1 mag/arcsec^2, are plotted in grey-scale.

4. Discussion

If the counter-streaming instability is indeed working in a sizable fraction of the dE,Ns to drive nuclei off-center, it is natural to ask why these dEs have counter-rotation in the first place. The first detections of counter-rotation in galaxy disks (Rubin *et al.* 1992; Merrifield & Kuijken 1994) lead to the hypothesis that the capture of gas with retrograde rotation and subsequent star-formation produced two counter-rotating stellar disks. This hypothesis predicts stellar populations of different ages and metallicities. Generally, the two disks will not have identical masses, so some net rotation is expected; this is, therefore, an unlikely explanation for FCC046.

Tremaine & Yu (2000) suggested that counter-rotation is produced when a triaxial halo with an initially retrograde pattern speed slowly changes to a prograde pattern speed. However, this situation probably does not occur very often. Moreover, this mechanism requires evolution on long timescales $\sim 10^{10}$ yr and hence requires dE,Ns to be old and unperturbed.

A more likely mechanism is the destruction of box-orbits, which are the backbone of any slowly rotating triaxial mass-distribution, by a growing nucleus. Stars on box orbits come very close to the nucleus and thus can be scattered into loop-orbits; conservation of angular momentum then requires that direct and retrograde loop orbits be equally populated (Evans & Collett 1994; Merritt & Quinlan 1998). If the nucleus has a mass larger than 2% of the total mass of the galaxy, evolution towards an axisymmetric shape requires a few crossing times ($\approx 10^7 - 10^8$ yr), while our simulations show that the counter-streaming instability develops on similar timescales. Late infall of gas (Conselice *et al.* 2003) (perhaps as a result of harassment (Moore *et al.* 1996; Mayer *et al.* 2001)) or globular clusters (Lotz *et al.* 2001) may be responsible for growing the nucleus. If this explanation holds, then the two counter-rotating stellar populations should have equal scale-lengths and chemical properties and nearly equal mass. Additionally, the nucleus may retain some of its initial angular momentum; we note that the nucleus of FCC046 is indeed rotating.

To summarize: using N-body simulations, we have shown that the counter-streaming instability is a viable explanation for at least the dE,N galaxy FCC046. The models can produce offsets as large as observed and successfully reproduce distinctive features in the surface photometry of FCC046, such as the oscillation of isophote centers. Although at the limit of what can reliably be extracted from the spectra, we find a tantalizing hint of counter-streaming in the major-axis spectra of this galaxy, which, however, needs to be corroborated at higher spectral resolution.

V.P.D. thanks the Sterrenkundig Observatorium for hospitality during an early stage of this project. We thank Stelios Kazantzidis and Anna Pasquali for useful discussions and the referee, Dr. O. Gnedin, for the suggested improvements.

REFERENCES

Adams, F. C., Ruden, S. P., Shu, F. H. 1989, ApJ, 347, 959

Barazza, F. D., Binggeli, B., & Jerjen, H. 2002, A&A, 391, 823

Binggeli, B., & Ferguson, H. C. 1994, A&A Rev., 6, 67

Binggeli, B., Barazza, F., Jerjen, H. 2000, A&A, 359, 447

Conselice, C. J., O'Neil, K., Gallagher, J. S., Wyse, R. G. 2003, ApJ, 591, 167

De Rijcke, S., Dejonghe, H., Zeilinger, W. W., & Hau, G. K. T. 2003, A&A, 400, 119

De Rijcke, S., Zeilinger, W. W., Dejonghe, H., & Hau, G. K. T. 2003, MNRAS, 339, 225

Evans, N. W., & Collett, J. L. 1994, ApJ, 420, L67

Geha, M., Guhathakurta, P., & van der Marel, R. P. 2003, AJ, 126, 1794

Gnedin, O. Y. , Zhao, H.-S., Pringle, J. E., Fall, S. M., Livio, M., & Meylan, G. 2002, ApJ, 568, L23

Levison, H. F., Duncan, M. J., & Smith, B. F. 1990, ApJ, 363, 66

Lotz, J. M., Telford, R., Ferguson, H. C., Miller, B. W., Stiavelli, M., & Mack J. 2001, ApJ, 552, 572

Mayer, L., Governato, F., Colpi, M., Moore, B., Quinn, T., Wadsley, J., Stadel, J., & Lake, G. 2001, ApJ, 559, 754

Merrifield, M. R., & Kuijken, K. 1994, ApJ, 432, 575

Merritt, D., & Quinlan, G. D. 1998, ApJ, 498, 625

Merritt, D., & Stiavelli, M. 1990, ApJ, 358, 399

Michielsen, D., De Rijcke, S., Dejonghe, H., Zeilinger, W. W., & Hau, G. K. T. 2003, ApJ, 597, L21

Miller, R. H., & Smith, B. F. 1992, ApJ, 393, 508

Moore, B., Katz, N., Lake, G., Dressler, A., & Oemler Jr., A. 1996, Nature, 379, 613

Rubin, V. C., Graham, J. A., & Kenney, J. D. P 1992, ApJ, 394, L9

Palmer, P. L., & Papaloizou, J. 1990, MNRAS, 243, 263

Phillipps, S., Drinkwater, M., Gregg, M., & Jones, J. 2001, ApJ, 560, 201

Prendergast, K. H., & Tomer, E., 1970, AJ, 75, 67

Rakos, K. & Schombert, J. 2003, accepted for publication by AJ, astro-ph/0312075

Sawamura, M. 1988, PASJ, 40, 279

Sellwood, J. A., & Valluri, M. 1997, MNRAS, 287, 124

Sellwood, J. A., & Merritt, D. 1994, ApJ, 425, 530

Sellwood, J. A. 1983, J. Comput. Phys., 50, 337

Taga, M., & Iye, M. 1998, MNRAS, 299, 111

Tremaine, S., & Yu, Q., 2000, MNRAS, 319, 1

Weinberg, M. D. 1994, ApJ, 421, 481

Zang, T. A., & Hohl, F. 1978, ApJ, 226, 521

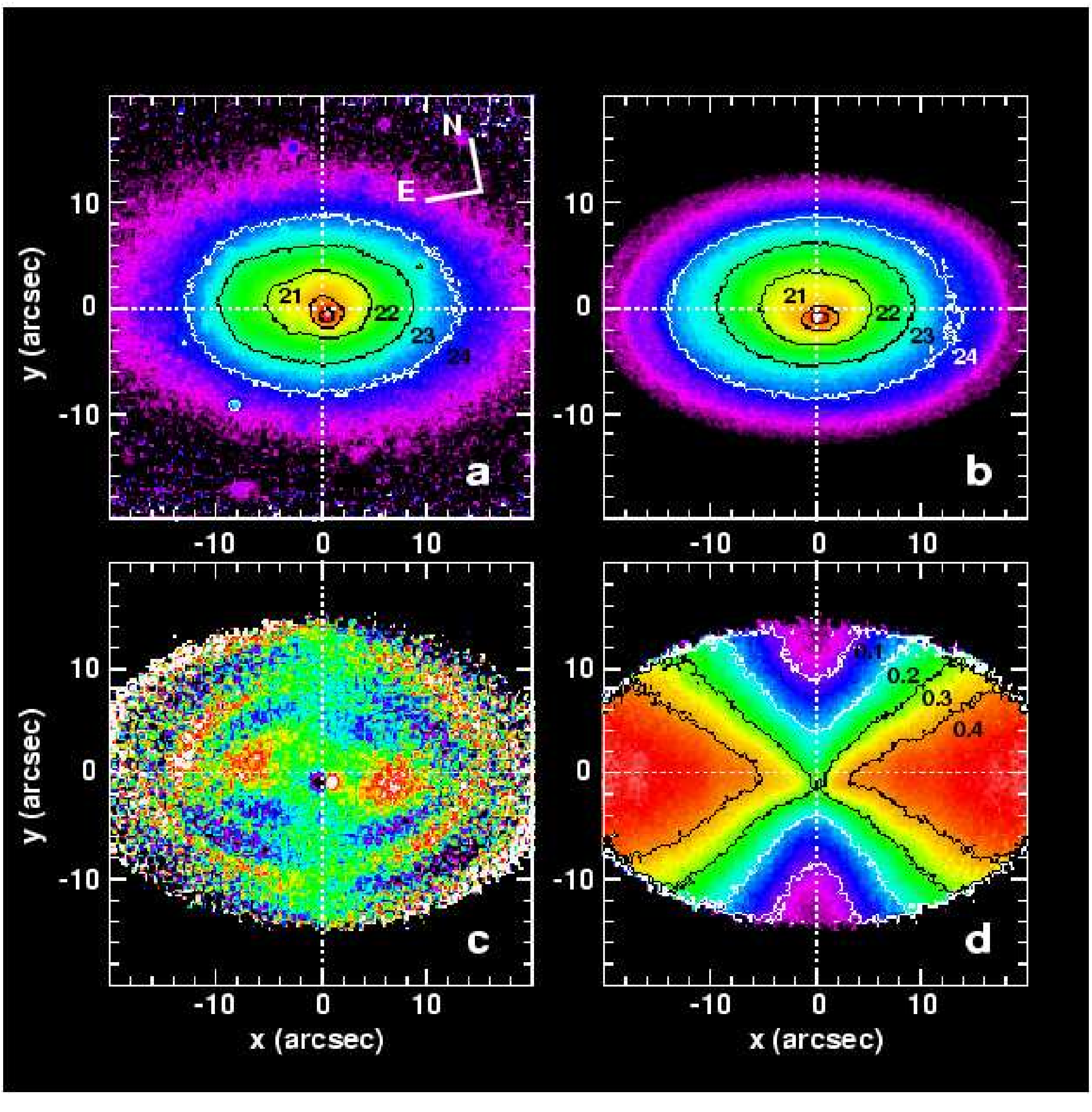

N
E
21
22
23
24
a
b
c
d
0.1
0.2
0.3
0.4
y (arcsec)
x (arcsec)
10
0
-10